

The Effect of Remaining Casting Skin on Cast Iron Components Fatigue Strength

^[1]Pawan Kumar Singh Nain

^[1]Department of Mechanical Engineering, Galgotias University, Yamuna Expressway Greater Noida, Uttar Pradesh

^[1]pawan.kumar@Galgotiasuniversity.edu.in

Abstract: The measurement of the fatigue power of casts with residual casting skin remains a problem. To date, the only consideration of the ruggedness of the casting skin during the design process was the reduction factor. Nevertheless, the consequence of discontinuities including inhomogeneous microstructures, imperfections, pores etc. is ignored by this reduction element. This work shows the rim zone of the cast, consisting of surface ruggedness and a deviating microstructure. In order to evaluate the effect of the casting skin on fatigue strength, fatigue experiments with deviating skin testers have been carried out on EN-GJS-400-15 and EN-GJS-700-2. In cyclical axial stress tests under alternation loading $R_r = -1$ on small flat specimens extracted from the rim zone, a cyclic conduct of the rim area microstructure was established. In addition, cyclical propensity tests were performed with alternating $R_5 = -1$ and pulsatory loading $R = 0$ in the integration of the findings from axial fatigue tests with an effect on surface roughness as well as stress gradients present in the casting components. The conclusions drawn from the study are translated into a formulation for a fatigue examination of the remainder of the casted tissue.

Keywords: Casting skin, Fatigue strength, Graphite degeneration, Nodular cast iron, SGI.

INTRODUCTION

Over the years, lightweight construction has gained increasing importance in reducing the weight in the manufacture and use of cars and automotive products to minimize CO₂ emissions. Alloys, for example aluminum and magnesium alloys, are often used to conserve weight. But these alloys are more expensive than cast iron and have less strength. Another way of reducing weight and keeping cast iron's beneficial properties is to scale it down. This can only be done if these components are kept safe and functional. For lightweight component design, therefore, the precondition is for better understanding of the cyclic content and fatigue behavior of cast iron components. The skin casting must nevertheless be considered during the design process to explain the fatigue actions of cast iron parts as accurately as possible, as

the development of casting skin during the casting process is natural and casting skin cannot always be avoided. Post-processing, such as the machining or shot peening of other casting materials, not only leads to higher costs, but cannot also be carried out on unreachable surfaces [1], [2]. To date the material conduct taken into account in existing design concepts is generally achieved by tests performed with machining specimens, and a reduction factor, such as the ruggedness factor $K_{R,r}$, in the FKM guideline is taken into account. The literature defines not only ruggedness on the surface but decarburization, or degeneration of graphite and the edges of ferritic or pearly. An investigation was carried out into cast skin fatigue components with the irremovable casting skin in order to assess the effect of casting on the fatigue behavior of EN-GJS-400-15 and EN-GJS-700-2 foundries. Casting processes were

subsequently designed to produce casting blanks for fatigue testing. Including bending specimens, flat specimens have been developed for axial strain research. To define the cyclical material properties for FE simulation, the findings obtained from the axial strain check. Only the findings of the bending experiments are discussed in this article.

During the research project Gusshaut, financed by the German Federation of Industrial Research Associations (AiF), the investigation and fatigue tests were conducted. A design principle is developed which takes into account the effect of casted skin on cast iron components' fatigue lives by drawing on the findings from fatigue studies [3], [4]. With fatigue testing on a cast iron part the definition is confirmed.

MATERIALS AND METHODS

Materials:

Skin casting is a natural effect resulting from the reaction of the melt with molding or core elements. Its most prominent forms of expression are the degenerated layer of graphite consisting of lamellae graphite's, formed because of the magnesium melt reaction with sulfur or oxygen from the molding, which means that nodular graphite's can no longer form. This project therefore contains 3 types of cast blanks, one with a surface only and two with rim zones consisting of a degenerated graphite sheet and a deviating microstructure, EN-GJS-400-15 and EN-GJS-700-2. Work on EN-GJS 400-15 (Table 1) in this paper.

A circular geometry casting was developed by the RWTH Aachen Foundry Institute for 14 blades of cast [Fig. 1]. Dross or erosion forming through a steady and smooth flow of melt was forbidden by the cast geometry gating method. At the edge of the cast between the melt and the sand core, the degenerate graphite coating forms [5]. Kutz is able to read a detailed description of the casting process.

Table 1: Overview of the casting blank type

| Type of casting blank | Bulk material | Rim zone | Surface roughness |
|-----------------------|---------------|---------------|-------------------|
| 1-PT_III | EN-GJS-400-15 | No | Yes |
| 2-GE_I | EN-GJS-400-15 | Pearlite, DGL | Yes |
| 3-GE_II | EN-GJS-400-15 | Ferrite, DGL | Yes |

Form 1 casting blanks (Table 1) were cast with only bulk material and surface ruggedness to discriminate between surface roughness effect and the rim region (Fig 1 top right). The impact of a changing microstructure along with the Degenerated Graphite layer (DGL) was examined by casting blanks of type 2 made of pearl-like graphite (GE I), and by casting blanks of type 3 made up of graphite lamellae in a ferritic matrix (GE II, Fig. 1.) [5]–[7]. In this analysis, the influence of the change was examined. Table 2 lists the chemical composition of the three cast blanks.

Table 2: Chemical composition of the EN-GJS-400-15 casting blanks (weight - %)

| Casting Type | C | Si | Mg | Cu | Mn | S | P | CE |
|--------------|-----|-----|------|-----|-----|-----|------|-----|
| 1-PT_III | 3.7 | 2.6 | 0.03 | 0.0 | 0.1 | 0.0 | 0.01 | 4.6 |
| 2-GE_I | 3.7 | 2.4 | 0.03 | 0.0 | 0.1 | 0.0 | 0.02 | 4.5 |
| 3-GE_II | 3.6 | 2.4 | 0.02 | 0.0 | 0.1 | 0.0 | 0.02 | 4.4 |

In comparison to the casts developed for this mission, EN-GJS-270 findings have been used because its micro-structure shows a pearl matrix with graphite lamellae that is similar to the rim / degenerated graphite layer micro-structure [3], [4], [8], [9].



Fig. 1. Produced casting blank geometry (top left), microstructure of EN-GJS-400-15 without rim with surface roughness - PT_III (top right), with rim of lamellar graphite in pearlitic matrix - GE_I (bottom left) and lamellar graphite in ferritic matrix - GE_II (bottom right)

Fatigue tests:

Fatigue tests on bending specimens (Fig. 2) with tensile $R_{\mu} = 0$ and alternating load $R_{\mu} = -1$ and under ambient air and room temperature have determined the effect of the casting skin on the fatigue life of casting components. Check fatigue on servo-hydraulic check plants (Fig. 3) with maximum power of 10 kN, until the specimen has a 20 per cent

loosened stiffness compared with the initial condition or until the target Nlim period number= 1 till 40 Hz is reached.

Specially for the testing of fatigue on surface areas, the clamping system ensures maximum stress on the surface of the specimen (with and without casting skin) [3]–[5], [7], [9]. The effect of casting skin on tiredness was examined by two styles of bending specimens from the bottom of the blank casting (Fig. 1, Fig. 2) with and without casting skin.

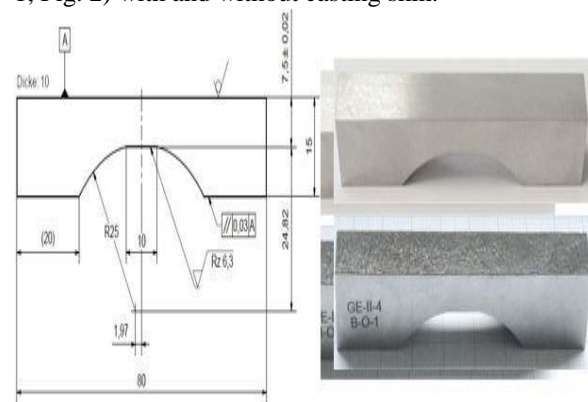


Fig. 2. Bending specimen geometry (left), bending specimen with machined surface (top right) and with casting skin (bottom right)

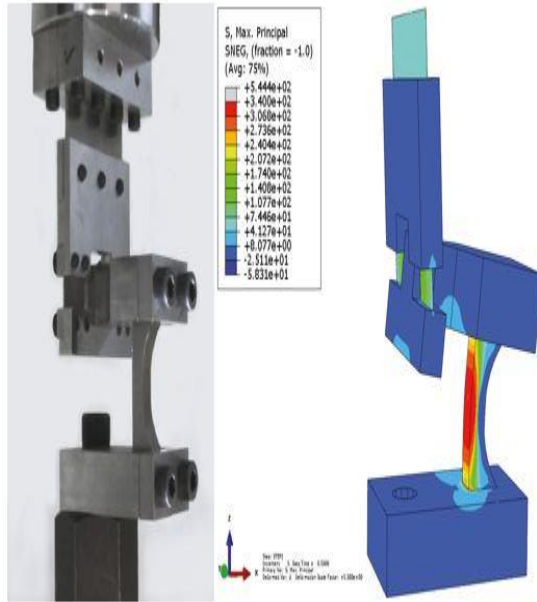


Fig. 3. Fatigue test setup (left) and FE-simulation (right) of the bending tests under two-point bending

RESULTS

The measurements of the tensile stress measures $R_{\mu=0}$ are shown in Fig. 4. The results are shown for EN-GJS-400-15, for a roughness or no-roughness comparison. The test results are analyzed by regression based on the maximum probability method which uses the least squares of the solution for determining the slope K of the low-cycle fatigue regime. This approach determines the curve parameters to minimize the sum of square curve deviations.

In low cycle fatigue, the difference in measurement is assumed to be consistent and will be adjusted until the limits of cycles $N_{G=1/107}$ for the high cycle fatigue. For this the pitch k^* must be specified in the high-cycle fatigue method [9], [10].

The scatter of the S-N curves for the bulk specimens is mathematically established: $T^{\approx} 1: 1.10$; $T^{\approx} 1: 1.13$ for specimens with rough surface. However, for cast iron products a scatter strip of 1:1.30 is recommended. For comparison, Table 3 lists the S-N curve parameters of all the curves displayed.

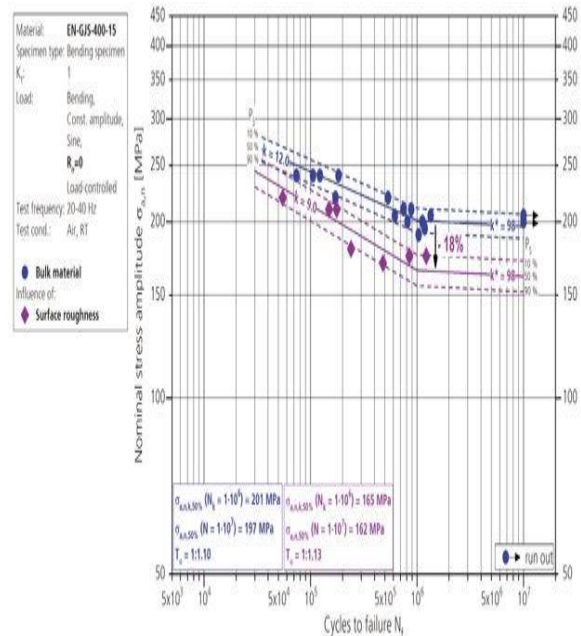


Fig. 4. Determined S-N curves of EN-GJS-400-15 specimen from the bulk and with preserved surface roughness

In contrast with the professionally machined specimens, the surface roughness of the bending specimen decreased the fatigue power by around 18 percent (Fig. 4). Sonsino's work shows that the fall in the decade following the knee stage for steel and cast iron parts would be 5 percent ($k^*= 44.9$). The evaluation of this project's test points indicates, however, that a k^* pitch= 2.5% per decade [11], [12].

Table 3: Overview over S-N curve parameter

| R=0 | K | N_k | σ_k (MPa) | T_k | Surface roughness | |
|----------------------|------|-------------------|---------------------|--------|-------------------|----------------|
| | | | | | Rz (μ m) | Ra (μ m) |
| EN-GJS-400-15 | | | | | | |
| Bulk material | 12.0 | $1 \cdot 10^6$ | 201 | 1:1.10 | 2.5 | - |
| Surface roughness | 9.0 | $1 \cdot 10^6$ | 165 | 1:1.13 | 65.7 ± 6.6 | 11.3 ± 1.1 |
| Run | 10.0 | $1 \cdot 10^6$ | 109 | 1:1.32 | - | - |
| EN-GJL-270* | | | | | | |
| Bulk material | 6.3 | $2.18 \cdot 10^5$ | 48 | 1:1.25 | - | - |
| FKM-modelline | | | | | | |
| Surface roughness | 5.0 | $1 \cdot 10^6$ | 166 | - | 80 | - |

* Rausch (2011)

A Hommel-Edamic ruggedness scan arm was used to

test surface ruggedness. Metallographic tests were performed on broken fatigue samples. Stereomicroscopy inspect the fracture surfaces and one of the fracture surfaces for chemical gravure were then removed from the specimen, extracted, ground and polished. The stereomicroscopy images were used to assess the fraction of each specimen's surface region with respect to the cross section of the specimen. The fracture surfaces were therefore subdivided into rim areas (red) and bulk surfaces (blue), each with a color (Fig. 5). Therefore, the rim zone proportions can be calculated and classified into four groups (Table 4). Specimens have been applied to the rim zone foothill group where the occurrence and distribution of cracks in the rim zone region reaches to more than the normal surface penetration depth.

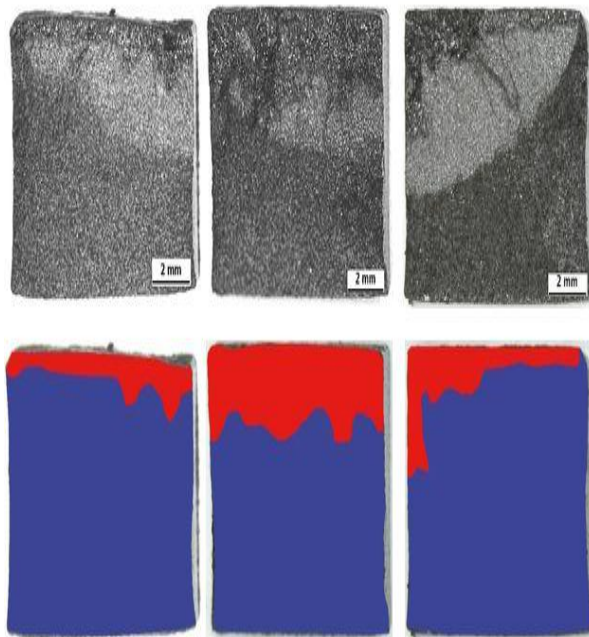


Fig. 5. Fracture surface with little (10 %, right) and higher (28 %, middle) rim proportion and rim zone foothill (left)

| Fraction of the rim zone on the specimens' cross section | | | |
|--|------------|----------|-------------------|
| Low [%] | Medium [%] | High [%] | Rim zone foothill |
| 2-11 | 12-21 | 22-31 | - |

Two types of microstructures (pearlitic: GE I and ferritic: GE II) in the randzone were tested, Table 1, in addition to the effect of degenerated graphite, the fatigue power of different microstructures was investigated. The analyses of the test results of the GE I and GE II castings indicate that in case of degenerated graphites the microstructure in the surface has a minor effect on their fatigue power. (Fig. 8). In Fig. 6 this is shown since it is not possible to distinguish between GE I S-N ($\tau_{n, k, 50\%} = 114$ MPa) and GE II ($\tau_{n, k, 50\%} = 111$ MPa) curves (table 3). The test points of the two castings were thus evaluated jointly (Fig. 7).

The only test points for exhaustion in Fig. 7 are coded by type of proportions of rim region (Table 4). The fatigue strength in the cross section of the bending specimen is decreased with an increasing fraction of the surface area. A rise in the proportion of the rim from low to high ($\tau_{n, k, 50\%} = 125$ MPa) ($\mu\text{m} / \text{s}$) leads to a reduction in fatigue strength of 24% (Table 4, Table 5). This reduces the fatigue strength by 24%.

Table 4: Rim zone proportion categorization of the specimen cross section

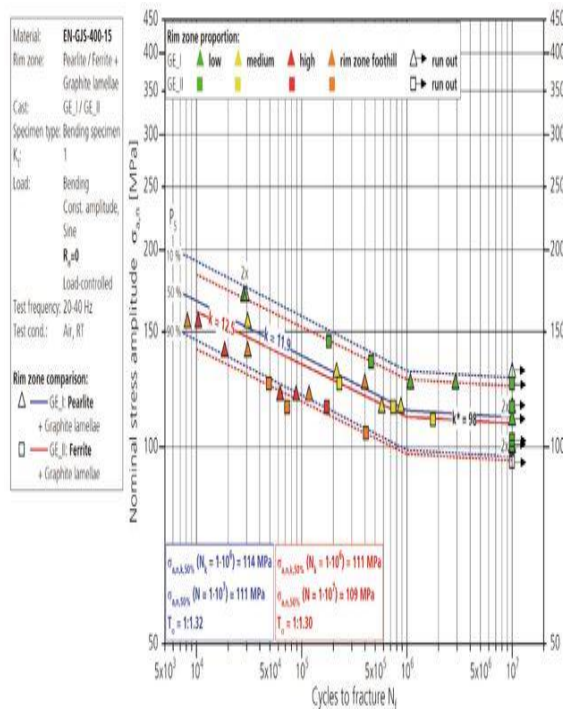


Fig. 6. Experimentally determined S-N curves of EN-GJS-400-15 specimen with a pearlitic (blue) and a ferritic (red) rim in the DGL

Comparing the S-N curves of the specimens with rim-zone graphite lamellae and surface-resilient specimens only (Fig. 1), the frequency of fatigue is decreased by 34% (Fig. 8, Table 3). Chart-Fig. 9 illustrates EN-GJS-400-15 and EN-GJL-270 differences in fatigue strength. The comparison of these S-N curves demonstrates that graphite lamellae are responsible for the proportional reduction of the tiredness in the rim zone. Due to a higher knot effect than the knotted graphite, the graphite lamellae in EN-GJL-270 have a less tiredness.

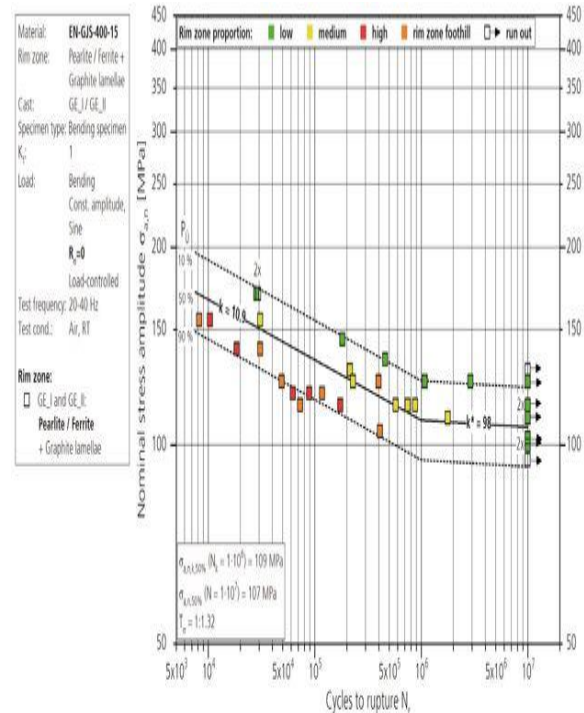


Fig. 7. Experimentally determined S-N curve of EN-GJS-400-15 specimens with a pearlitic and a ferritic rim in the DGL

Table 5: Nominal stress amplitude $\sigma_{a,n}$ at the knee point $N_k = 1.106$ depending on the rim zone proportion

| | Rim zone dependent nominal stress amplitude | | |
|--|---|---------|---------|
| | 2 - 11 | 12 - 21 | 22 - 31 |
| $\sigma_{0.2,50\%}(N_k = 1 \cdot 10^6) [\text{MPa}]$ | 125 | 109 | 95 |

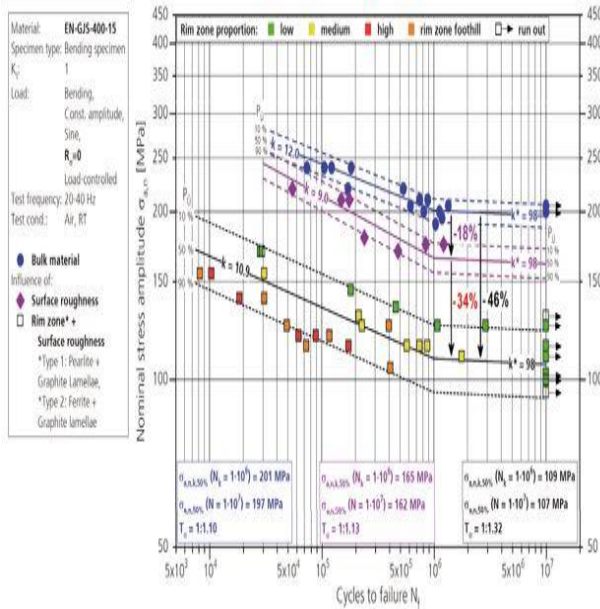


Fig. 8. Comparison of experimentally determined S-N curves of EN-GJS-400-15 specimens being completely machined, with only surface roughness and with a pearlitic or a ferritic rim in the DGL

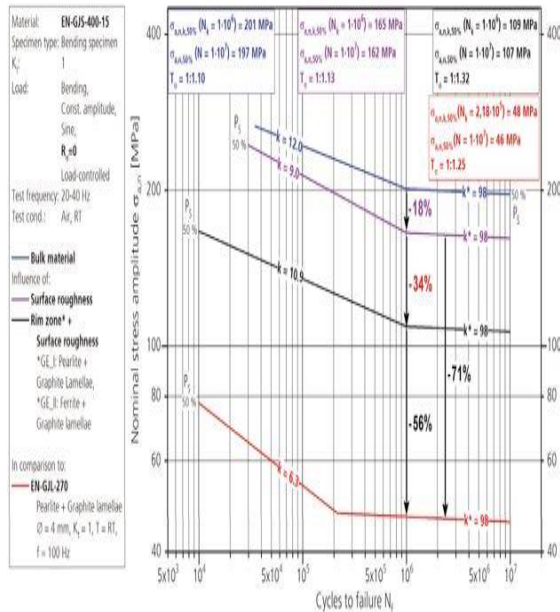


Fig. 9. Experimentally determined S-N curves of EN-GJS-400-15 specimens being completely machined, with only surface roughness and with a pearlitic or a ferritic rim in the DGL in comparison with results for an EN-GJL-270

The FMM guideline [FKM (2012)] is used to calculate and plot the S-N curve for EN-GJS-400-15 with surface roughness (Fig. 10) using a rugging factor set out in accordance with the Guideline (Table 6) because the fatigue life of cast iron components is usually estimated.

Table 6: Parameter for calculation of roughness factor KR, σ according to FKM-guideline

| | Parameters for calculation of $K_{R,\sigma}$ | | | | |
|---------------|--|----------------------------|---------------------|--------------------------|-----------------------|
| | R_m [MPa] | $\sigma_{R,\sigma}$ [-] | R_z [μ m] | $R_{m,N_{lim}}$ [MPa] | $K_{R,\sigma}$ [-] |
| EN-GJS-400-15 | 400 | 0.16 | 80 | 400 | 0.91 |

Table 3 shows that the knee point ratio n, calculated in accordance with FKM guideline for the EN-GJS-400-15, is comparable, n of a surface-roughness specimen. In both S-N curves only the direction k deviates from the cyclic material compoment obtained and the fatigue power in the cycle-low fatigue regime is thus overestimated. The picture. 10 shows that FKM cannot properly represent the data received and overestimates also the tiredness determined by graphite degeneration on fatigue specimens. In this instance the nominal knee point stress amplitude $Nk=15-06$ derived from the FKM Guideline, more precisely the nominal surface rugged specimens (T_a , n, k, 50 percent = 165 MPa). In these cases the rare stress amplitude is $\bar{\sigma}$, n, k = 166 MPa.

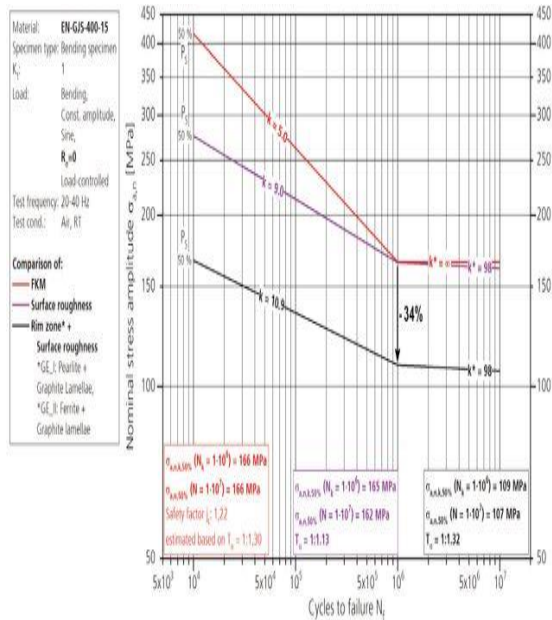


Fig. 10. Comparison of the experimentally determined S-N curves of EN-GJS-400-15 for the specimens with surface roughness only, with a pearlitic or a ferritic rim and a S-N curve calculated according to the FKM guideline

DISCUSSION

Next, the surface roughness that is preserved decreases fatigue strength in contrast to the fully treated EN-GJS-400-15 specimens as expected (Fig. 4). In fact, the DGL graphite lamellae adversely affect the degree of fatigue. On the other hand, it makes no difference whether this is pearlitic or ferritic as far as the microstructure of the DGL matrix is concerned. Due to the high internal nodal effect on sharp lamal graphite the negative effect of the graphite lamellae seems to be superpose to fatigue strength by a stronger pearl microstructure (Fig. 6, Fig. 7). This effect is the reason why lamellar cast iron has a less fatigue strength compared to nodular cast iron (Fig. 9). The FKM manual has a large database, but fails to take account, suggesting a deviating micro structure, of the effect of casting skin on fatigue power in its entirety. This difference between guidance and experimental results has led to the study of various skin condition casting and combinations of bulk material.

CONCLUSION

The findings presented in the present paper show that casting skin is not only a ruggedness of the surface but also a combination of degenerography and microstructural modifications in addition to surface ruggedness. Therefore, it is not only important to study the cyclic tiredness properties of the bulk casting material but also of the entire layer system consisting of surface roughness, degenerations of graphite and deviating microstructural elements. Further work into the EN-GJS-700-2 and its effect on the fatigue power of casting skin-containing specimens also requires experiments in this research. This study includes FE simulations are also performed to establish a model of fatigue evaluation based on the results of cyclic fatigue experiments and the cyclical material properties calculated by strain-controlled fatigue testing on flat specimens on small scales under axial, alternating loading. An evaluation definition to determine the local fatigue strength of nodular cast iron components in rim areas requires all details. A cast iron part made of nodular cast iron shall be simulated and fatigue measured at the end of the project to verify the accuracy of this fatigue calculation formulation.

REFERENCES

1. M. Shirani and G. Härkegård, "Large scale axial fatigue testing of ductile cast iron for heavy section wind turbine components," Eng. Fail. Anal., 2011.
2. S. Boonmee and D. M. Stefanescu, "Occurrence and effect of casting skin in compacted graphite iron," Int. J. Cast Met. Res., 2016.
3. S. Nasu, S. Fujita, N. Furusato, S. Yamada, and S. Hiratsuka, "Effect of casting skin condition on fatigue strength of gray cast iron," in 72nd World Foundry Congress, WFC 2016, 2016.
4. S. Boonmee and D. M. Stefanescu, "International Journal of Cast Metals Research Occurrence and effect of casting skin in compacted graphite iron Occurrence and effect of casting skin in compacted

**International Journal of Engineering Research in Computer Science and Engineering
(IJERCSE)**

Vol 4, Issue 11, November 2017

- graphite iron,” *Int. J. Cast Met. Res.*, 2016.
5. K. Bergner, C. Bleicher, and R. Wagener, “Influence of remaining casting skin on the fatigue strength of cast iron components,” in *Procedia Structural Integrity*, 2019.
6. S. Nasu, S. Fujita, N. Furusato, S. Yamada, and S. Hiratsuka, “Effect of casting skin condition on fatigue strength of gray cast iron,” *Int. J. Met.*, 2017.
7. A. Szczotok, N. Radek, and R. Dwornicka, “Effect of the induction hardening on microstructures of the selected steels,” in *METAL 2018 - 27th International Conference on Metallurgy and Materials, Conference Proceedings*, 2018.
8. G. Nicoletto and E. Riva, “Fatica ad alta temperatura e ad alto numero di cicli di leghe di alluminio per applicazioni motoristiche,” *Metall. Ital.*, 2011.
9. S. Boonmee, “Ductile and Compacted Graphite Iron Casting Skin -- Evaluation, Effect on Fatigue Strength and Elimination,” 2013.
10. S. Biswas and C. Monroe, “Identifying Cast Iron Microstructure Variation Using Acoustic Resonance Techniques,” *Int. J. Met.*, 2019.
11. J. W. Soedarsono, B. Suharno, and R. D. Sulamet-Ariobimo, “Effect of casting design to microstructure and mechanical properties of 3 mm TWDI plate,” in *Advanced Materials Research*, 2012.
12. L. Tian, Z. Li, Q. Ke, E. Jin, and S. Dong, “Nondestructive testing and pull shear performance experiment on bionic heterogeneous compound materials interface,” *Nongye Gongcheng Xuebao/Transactions Chinese Soc. Agric. Eng.*, 2015.
13. VM Prabhakaran, S Balamurugan, S Charanyaa, “Sequence Flow Modelling for Efficient Protection of Personal Health Records (PHRs) in Cloud”, *International Journal of Innovative Research in Computer and Communication Engineering*, 2015
14. RS Venkatesh, K Deepika, R Poornima, S Balamurugan, M Sowmiya, “A Novel Dynamic Object Oriented Model for Automated Credit Card Management System”, *International Journal of Innovative Research in Science, Engineering and Technology* , Vol. 4, Issue 2, February 2015
15. R Santhya, S Latha, S Balamurugan, S Charanyaa, “Certain Investigations on Methods Developed for Efficient Discovery of Matching Dependencies” *International Journal of Innovative Research in Computer and Communication Engineering* , Vol. 3, Issue 1, January 2015